ACS NANO
www.acsnano.org
ARTICLE

Charge Carrier Inversion in a Doped Thin Film Organic Semiconductor Island

Zeno Schumacher,* Rasa Rejali, Megan Cowie, Andreas Spielhofer, Yoichi Miyahara, and Peter Grutter

Cite This: ACS Nano 2021, 15, 10377−10383
Read Online

ACCESS | Metrics & More | Article Recommendations | Supporting Information

ABSTRACT: Inducing an inversion layer in organic semiconductors is a highly nontrivial, but critical, achievement for producing organic field-effect transistor (OFET) devices, which rely on the generation of inversion, accumulation, and depletion regimes for successful operation. Here, we develop a pulsed bias technique to characterize the dopant type of any organic material system, without prior knowledge or characterization of the material in question. We use this technique on a pentacene/PTCDI heterostructure and thus deduce that pentacene is exhibiting *n*-doped like response. The source of the additional charges in the pentacene island can be identified by charging rings in the dissipation channel of the noncontact atomic force microscopy (AFM) signal, a typical signature for localized charge transfer from the AFM tip to the sample. Additionally, through tip-induced band-bending, we generate inversion, depletion, and accumulation regimes over a 20 nm radius, three monolayer thick *n*-doped pentacene island. Our findings demonstrate that nanometer-scale lateral extent and thickness are sufficient for an OFET device to operate in the inversion regime.

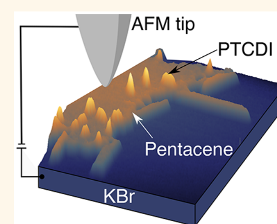

KEYWORDS: *organic field transistor, AFM, small organic molecules, KPFM, pentacene, thin film*

Downloaded via MCGILL UNIV on June 28, 2021 at 17:27:07 (UTC).
See https://pubs.acs.org/sharingguidelines for options on how to legitimately share published articles.

Currently, of the few tools available to investigate charge transport and carrier generation at the nanoscale, the most versatile and powerful is the combination of noncontact atomic force microscopy (nc-AFM) and Kelvin probe force spectroscopy (KPFS): the former provides structural information, while the latter allows for measuring charge distribution. KPFS is a measurement of the contact potential difference between the AFM tip and the sample, and so, can be used to detect surface potential changes that occur when a semiconductor is illuminated.[1−8] The combination of these techniques help to understanding the fundamental physics and properties of nanoscale electronics, and has been used to measure the charge state of individual molecules.[9]

Nc-AFM can be used to directly measure the force gradient between the tip and sample. In the small oscillation amplitude limit for the familiar metallic tip-metallic sample case, the electrostatic force, F_{elec}, can be related to the measured frequency shift, Δf, as follows

$$\Delta f \propto \frac{\partial F_{\mathrm{elec}}}{\partial z} = \frac{1}{2}\frac{\partial^2 C_{\mathrm{ts}}}{\partial z^2}(V_{\mathrm{DC}} - V_{\mathrm{CPD}})^2 \quad (1)$$

where C_{ts} is the tip−sample capacitance, V_{DC} the applied bias voltage, and V_{CPD} the contact potential difference. Usually, the tip−sample capacitance is assumed to be independent of the applied voltage, and for many doped semiconductor systems studied by nc-AFM, this is a good approximation, even though the capacitance is strictly a function of the applied voltage in these cases.[10,11]

A more rigorous treatment considers that the capacitance of a doped semiconductor varies as the applied voltage is increased. In a doped semiconductor, band bending at the surface and the formation of depletion and inversion layers within the penetration-depth lead to this voltage-dependent capacitance.

There is clear dissonance between the above-stated physical picture and the common analytical assumption that the tip−sample capacitance is voltage-independent.[12] The solution lies in noting that the effects of a voltage-dependent capacitance are, in most systems, quite benign. The tip-induced band bending in the semiconductor needs to be strong enough to achieve depletion or even inversion. The tip-induced band bending is a function of applied bias voltage, tip−sample distance, tip radius, as well as semiconductor parameters such as doping concentration.[13,14] Therefore, only for the right set of these parameters depletion can be achieved, resulting in a change in the tip−sample capacitance. Furthermore, it is necessary to record the full V_{DC} bias response of the system to observe the effect of the voltage dependent capacitance. As such, the popular Kelvin probe force microscopy (KPFM) technique is not appropriate for this application, as it only

Received: March 26, 2021
Accepted: May 25, 2021
Published: May 28, 2021

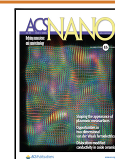

© 2021 American Chemical Society
https://doi.org/10.1021/acsnano.1c02600
ACS Nano 2021, 15, 10377−10383

records the contact potential difference between the tip and the sample (i.e., the maximum of the parabola and not the curvature).

Theoretical work on understanding the fundamental physics of doped semiconductors probed by AFM was published in the 1990s.[11,15,16] Experimental verification of the theorized behavior was published several years later, when the accumulation, depletion, and inversion regimes in a *n*-doped InAs sample were measured using AFM.[17]

RESULTS AND DISCUSSION

In this study, we thermally deposit 0.4 monolayer of pentacene on an *in situ* cleaved KBr crystal, followed by evaporation of 0.2 monolayer of 3,4,9,10-perylenetetracarboxylic diimide (PTCDI). KBr was chosen since it is a well studied insulator and substrate for molecular growth. Even though bulk KBr will not allow for a back electrode and therefore lead to subtle difference to a MIS structure (discussed later), the system allows to study molecule charging and doping responses. In general, pentacene grows in large, flat islands on KBr and stands upright, with the plane and the long axis of the molecule perpendicular to the substrate surface, or with the plane of the molecule perpendicular to slightly tilted and the long axis parallel to the surface.[18] Thus, for a measured height of approximately 2.1 nm, we expect the pentacene islands are three monolayers thick, assuming the molecular long axis is parallel and the plane of the molecule perpendicular to the surface. PTCDI, on the other hand, grows on KBr substrates to form longer, needle-shaped islands.[19] As such, pentacene and PTCDI are easily distinguishable in topographic images. Together pentacene and PTCDI form heterostructures of small PTCDI islands at the edges or on top of large pentacene islands. Pentacene together with PTCDI derivatives have previously been used as model structures for ambipolar OFET,[20] while *n*-type interfacial doping was achieved in pentacene as well.[21] A pentacene based OFET was made to successfully operate in the inversion-mode.[22] A topography image, recorded in constant frequency shift mode, is shown in Figure 1(a); simultaneously acquired frequency modulation-(FM)-KPFM data is shown in Figure 1(b).

We perform KPFS on a pentacene/PTCDI heterostructure (the location is indicated in Figure 1(c) by a red cross) as shown in Figure 2(a) (recorded at 0 nm tip lift from $\Delta f = -10$ Hz set point). The frequency shift is not parabolic as a function of applied bias as expected from eq 1, indicating a non-negligible voltage-dependence in the capacitance as expected in a doped semiconductor.[11,15]

In fact, the capacitance in a metal−insulator−semiconductor (MIS) structure—physically represented by a metal AFM tip probing a semiconductor sample—exhibits three distinct regimes: accumulation, depletion and inversion. Consider a *n*-doped sample interacting with a positively biased tip: the mobile electrons in the sample are attracted to the sample surface, resulting in an accumulation layer of the majority carriers (electrons, in this case). Under negative tip bias, the majority carriers are repelled from the sample surface, leading to a depletion layer. An increasingly negative bias leads to a thicker depletion layer until the minority carrier density at the surface surpasses the initial majority carrier density, as a result of increasing band bending, leading to an inversion layer.[17,23] A similar understanding applies to *p*-doped semiconductors.

As such, to better probe the nonparabolic response in Figure 2(a), the numerically differentiated frequency shift with respect to the applied tip bias is plotted. The derivative is not linear over a −6 to 8 V bias range. Instead, the derivative is comprised, piece-wise, of three lines with distinct slopes.

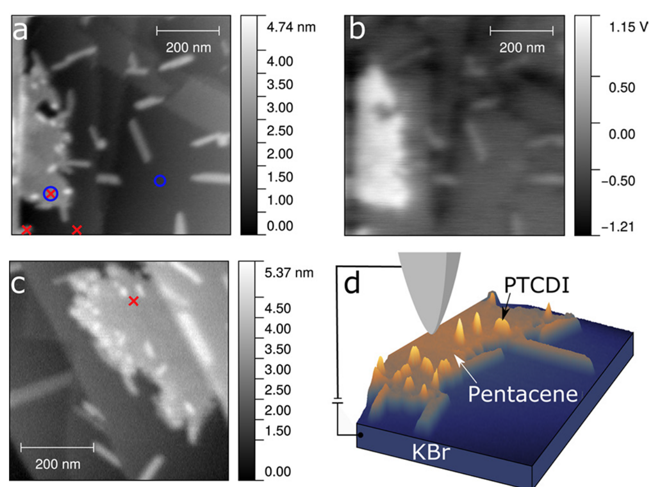

Figure 1. (a) Topography image of PTCDI on a pentacene island, on top of a KBr substrate (oscillation amplitude, A = 6 nm, frequency shift set point, Δf = −6 Hz). (b) Simultaneously acquired frequency modulation KPFM image (frequency and amplitude of the ac modulation: 600 Hz and 1 Vpp). (c) Topography image of an additional measurement site (A = 6 nm, Δf = −10 Hz). Red crosses and blue circles indicate locations of spectroscopy or pulsed measurements, respectively. (d) Graphical illustration of the measurement setup.

We use the model presented by Hudlet *et al.*[11] which includes the voltage dependent capacitance to calculate the electrostatic force between a metal tip and a doped semiconductor as shown in Figure 2(b). We add a parabolic frequency shift to the calculated signal to account for the capacitive force between the body of the tip and the sample as well as any background effects due to the KBr substrate. The asymmetric shape of the bias spectroscopy measurement on pentacene can be qualitatively reproduced, emphasizing the need to consider the voltage dependent capacitance for our system. Despite the fact that the band bending and carrier diffusion in our system is essentially 3-dimensional, the qualitative agreement between the measurement and the model calculation that assumes one-dimensional (plane−plane) system is notable. The difference in the slope of the derivative is not fully reproduced with this simple model, which we attribute to different carrier recombination times, unknown doping concentration, tip−sample capacitance, and neglected substrate effects. Lower intrinsic carrier densities and frequency shift as a function of surface potential are shown in the SI.

The spatial variation of the nonparabolic KPFS data is illustrated in Figure 3. We take the absolute difference of the fitted derivative of the frequency shift ($d\Delta f/dV$) obtained for individual fits to the positive and negative voltage window of the KPFS data (details in SI). The pentacene island exhibits a strong difference, with some variation within, while the PTCDI islands connected to it (red circles) do not show a significant difference and behave more in line with the KBr substrate. This indicates the doped semiconductor response is limited to the pentacene island.

Pulse Bias Probe for Dopant Type Identification. It is well-known that the capacitance of an MIS structure operating

https://doi.org/10.1021/acsnano.1c02600
ACS Nano 2021, 15, 10377−10383

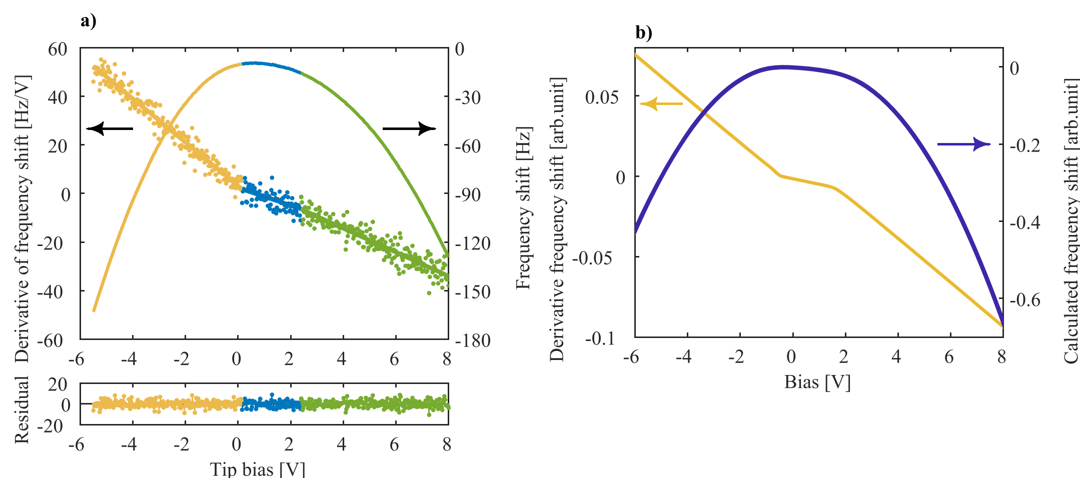

Figure 2. (a) KPFS measurement on a pentacene/PTCDI heterostructure. A clearly nonparabolic response is observed. The numerically differentiated frequency shift with respect to the applied bias is fitted to a straight line from the positive(green)/negative(yellow) side until the fit is optimized. The center (blue) is fitted with a straight line between the end points of the respective fits. The residuals are shown below. (b) Calculated frequency shift for a doped semiconductor-metal tip system based on ref 11. An intrinsic carrier density of $10^2(\mathrm{cm}^{-3})$, a dopant density of $(5 \times 10^{15}\mathrm{cm}^{-3})$, a mean tip−sample distance of 5.5 nm and an oscillation amplitude of 9 nm was used.

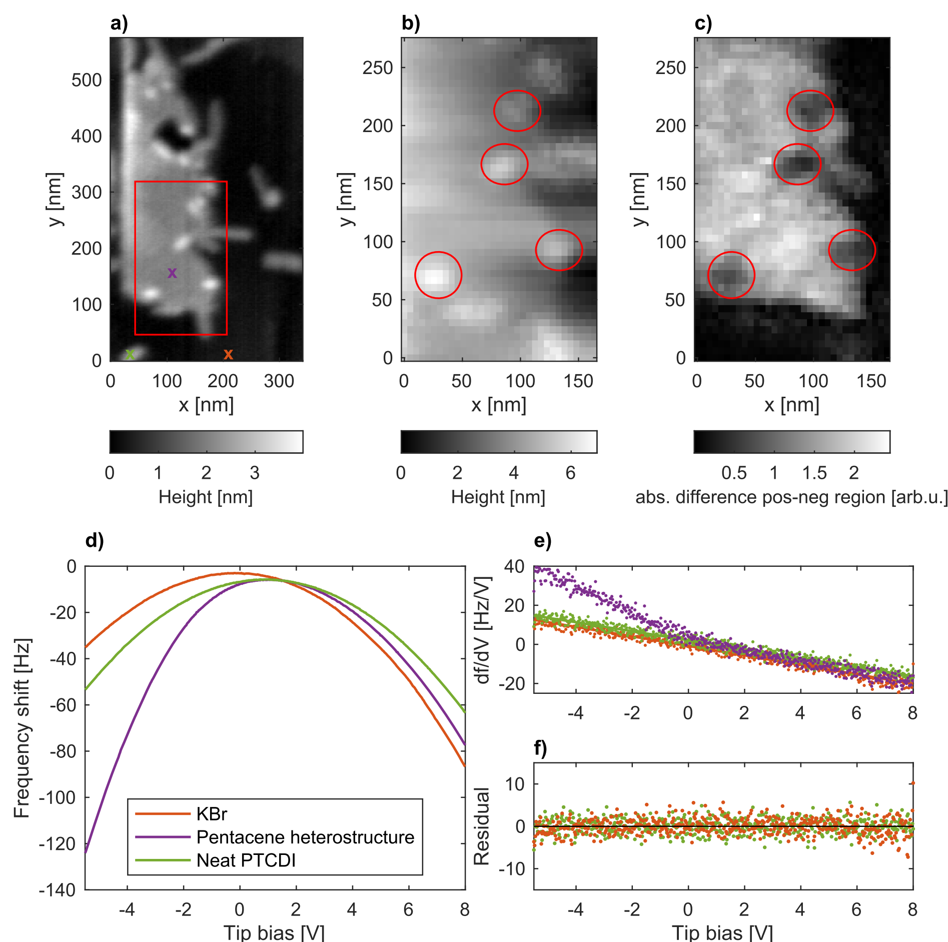

Figure 3. (a) Topography image indicating the location of the KPFS map with a red square, as well as the locations of the KPFS point spectra (d) with the respective colored crosses. (b) Topography extracted from a KPFS map of pentacene/PTCDI island. (c) The difference in the derivative of the frequency shift for the positive and negative bias side clearly shows a difference for the pentacene island while no significant difference is observed for the KBr crystal and the PTCDI islands (red circle) connected to the pentacene island. (d) KPFS measurements on KBr, doped pentacene, and neat PTCDI. The derivative of the frequency shift (e) reveals linear behavior for KBr and neat PTCDI, indicating parabolic behavior of the frequency shift. The doped pentacene does not show a linear behavior. (f) The residual to a linear fit for KBr and neat PTCDI (red and green) is shown at the bottom. All data recorded at 0 nm tip lift from $\Delta f = -6$ Hz set point at a bias of 1.3 V.

https://doi.org/10.1021/acsnano.1c02600
ACS Nano 2021, 15, 10377−10383

in the inversion regime exhibits a frequency dependence, whereas the capacitance in the accumulation-mode does not.[23,24] In fact, pulsed MIS capacitance measurements have previously been used to determine the minority carrier lifetime in bulk samples.[25−30] To this end, we use a pulsed bias experiment to verify whether the sample is *n*-doped or *p*-doped (see Methods).

No significant change in frequency shift is observed for KBr for both positive and negative applied square waves, as expected. The pentacene/PTCDI heterostructure, on the other hand, exhibits a decrease in frequency shift with increasing pulse frequency for negative voltages. A decreased response for higher pulse frequencies is expected for inversion due to the finite life- and generation-time of the minority carriers needed to form the inversion layer. We can deduce that the inversion regime occurs for negative bias, which in turns corresponds to *n*-doped pentacene. As such, we can assign the three regimes identified in Figure 2(a) to inversion (yellow), depletion (blue), and accumulation (green). The plateau reached at positive bias for the pentacene location can be attributed to the small contribution of minority carriers due to the starting point (1 V) of the pulsing being located in the depletion regime.

The exact lifetime of the minority carriers cannot be extracted from this measurement, since the exact doping concentration is unknown, this must be a known parameter for a quantitative result to be extracted from the pulsed MOS capacitance measurement presented by Zerbst.[25] However, it can be concluded that the life- or generation-time of the minority carrier is in the order of tens of microseconds corresponding to a $1/e$ decay time in our measurements.

Furthermore, we must consider the subtle differences between the doped semiconductor measured here, and a MIS structure. For example, in contrast to a MIS field effect transistor (MOSFET), where the minority carriers are injected by the metal contact, no direct electrical connection between the doped semiconductor to the metal electrode exist in our system. The minority carriers needed to form the inversion layer are, in fact, supplied by the larger pentacene/PTCDI island. Only the area directly underneath our AFM tip is depleted of majority carriers. The time response in Figure 4 could therefore be limited by the minority carrier generation and diffusion in contrast to just the minority carrier lifetime.

A schematic drawing of the experimental configuration of tip and sample can be seen in Figure 5. The corresponding band diagram, for a system consisting of a metal (AFM tip), insulator (vacuum), semiconductor (pentacene and PTCDI heterostructure), insulator (KBr substrate), and metal back electrode (sample holder) is also illustrated. As shown in Figure 5(a), the electric field penetration range is confined to the area underneath the AFM tip. This implies the carriers density directly under the tip are exclusively altered by the incident electric field. For further illustration, we consider a simulation of the hole and electron concentration for a *n*-doped (10^{16} cm^{-3}) 2.5 nm thick Si sample, on top of a 100 nm insulator ($\epsilon = 4.1$) supported by a metal electrode (0 V) with a top electrode (20 nm radius as specified by manufacturer) separated by 3 nm of vacuum (Figure 5(b). It is clear that only the area beneath the top electrode (tip) is inverted when a negative bias is applied. The hole concentration surpassed the initial dopant concentration at a bias of −10 V, therefore inverting the semiconductor underneath the tip to a *p*-type.

Origin of Doping Response. Theoretically, a non-parabolic response should only be observed over the doped

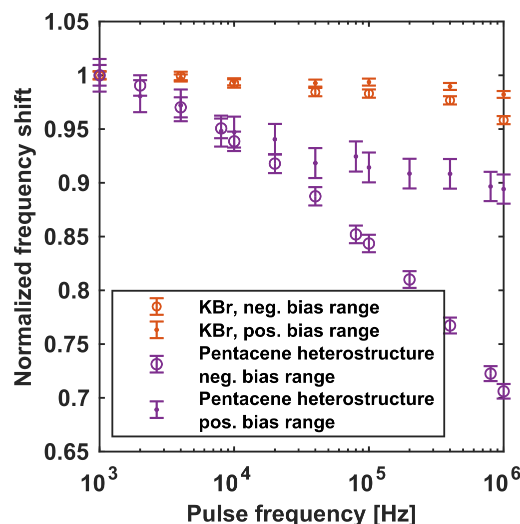

Figure 4. A square wave voltage is applied to the tip and the frequency shift is recorded for a tested frequency range from 1 kHz to 1 MHz. The frequency shift is normalized to the lowest applied pulse frequency. Pentacene heterostructure (purple) exhibits a strong frequency response in the negative bias range/inversion (open circle) where as KBr (red) shows no response. In the positive bias range/accumulation (full dots) a response is measured, reaching a plateau after 10 kHz.

semiconductor; measurements taken over neat PTCDI and KBr should reveal purely parabolic behavior as a function of bias, as indicated by eq 1. Thus, we repeat the same KPFS measurements over clean KBr and neat PTCDI, and compare the results with data taken over the pentacene/PTCDI heterostructure (shown in Figure 3). The respective measurement locations are indicated in Figure 1(a) by three red crosses. As expected, we observe that frequency shift measurements taken over KBr and neat PTCDI are parabolic. Accordingly, the derivative of the frequency shift is purely linear over the applied bias range for the aforementioned data sets. In contrast, KPFS measurements taken over pentacene/PTCDI heterostructure show the same nonparabolic behavior as before. The same experiment was repeated with different cantilevers (with a new Pt−Ir coated cantilever (PPP-NCHPt) and a silicon cantilever (PPP-NCHR)) for isolated, separate pentacene/PTCDI islands, all to reveal the same results.

While it might appear as if the *n*-doping behavior of the pentacene layer is due to the PTCDI islands, we have found nonparabolic behavior in neat pentacene islands as well. A common feature for all island exhibiting a doped semiconductor response are individual charging sites located in the respective pentacene islands. These charging sites appear as rings in the dissipation signal of the AFM (see SI), indicating a charge transfer from the tip to the sample.[31,32] Charging of pentacene and other adsorbed molecules has previously been demonstrated with AFM at low temperatures.[9,33,34] While the nature of these sites is of great interest and under investigation, this publication focused on the global effect of these charging sites on the pentacene layer. KPFS measurements on neat pentacene before the deposition of PTCDI follow a parabolic behavior (see SI), as long as there are no charging rings in the dissipation channel, confirming our conclusion of these charging sites acting as the donor for adding charges to the pentacene island and thereby provoking the *n*-doping response we observe. We estimated a dopant density based on the

https://doi.org/10.1021/acsnano.1c02600
ACS Nano 2021, 15, 10377−10383

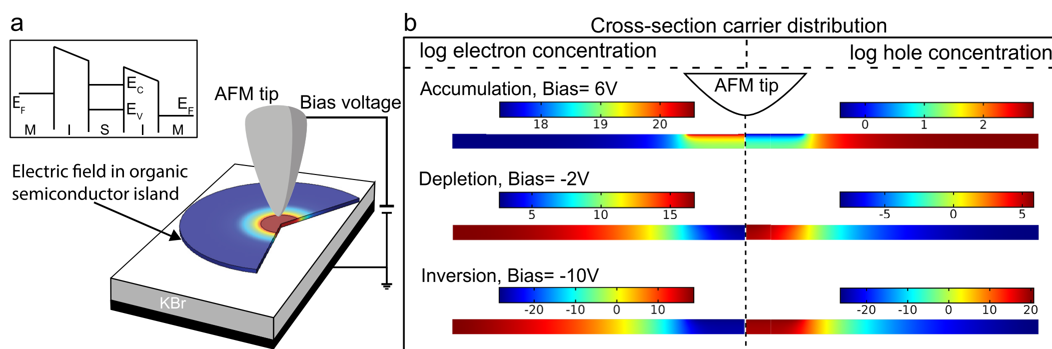

Figure 5. (a) A schematic of the experimental setup. The color-scale of the semiconductor corresponds to the electric potential in the sample at a bias voltage of −10 V. The inset shows a band diagram of the sample structure with a organic semiconductor sandwiched between two insulators, followed by a metal contact. (b) Cross section of a finite element simulation, done using COMSOL, of the hole and electron concentration in a *n*-doped (10^{16}cm^{-3}), 2.5 nm thick Si sample, as shown on the left. Only the area underneath the tip is inverted when a positive bias is applied.

number of charging site per pentacene island. By taking the amount of charging rings observed as the number of dopants per island, a dopant concentration for the island present above of 5×10^{16} cm^{-3} was obtained. We identify five charging rings (see SI) and a volume of 10^{-16} cm^3 = 400 nm × 120 nm × 2.1 nm for the pentacene island, resulting in a reasonable dopant density where we would expect to observe the doped semiconductor response.

CONCLUSION

In conclusion, we measure the electrostatic force of an accumulation, depletion, and inversion layer in a 2.1 nm thick organic semiconductor. Charging sites in the pentacene island, showing up as rings in the dissipation channel, act as a dopant for the much larger pentacene island, resulting in a *n*-doped pentacene island. The inversion layer is generated by sweeping the bias voltage on an AFM tip, which is in close proximity to the island. Only the area directly underneath the AFM tip (approximate radius of 20 nm) is depleted of majority carriers. The measurement qualitatively agrees with numerical simulations. Exact numerical calculations are not possible for our system, since various parameter such as the dopant concentration, intrinsic carrier density, KBr capacitance contribution, *etc.* are unknown.

The formation of the inversion layer was further verified by applying a pulsed voltage and measuring the frequency response. Observing the movement of carriers in organic semiconductor and the formation of inversion layer at this length scale is a crucial step toward studying organic photovoltaics at the nanometer scale. Our study shows that a 2.1 nm thick *n*-doped pentacene layer can locally be brought to inversion at an approximate 20 nm lateral size. This would enable the production of an organic FET with a channel on the same length scale. Further investigation of this system under light illumination is of great interest to advance the understanding of the local nanometer behavior of organic semiconductor during charge generation. Experiments conducted under illumination could potentially help to determine the minority carrier generation- and lifetime of organic semiconductors at the nanometer scale.

METHODS

All AFM measurements were performed on a JEOL JSPM-4500A ultra high vacuum (UHV) cantilever based beam deflection AFM setup with a base pressure of <3×10^{-10} mBar at room temperature. Commercial metal coated silicon cantilevers were used for all measurements (Nanosensors, PPP-NCHPt). A Nanonis OC4 system is used for control and recording of the AFM signal.

Sample Preparation. The KBr crystal were cleaved *in situ* in our UHV chamber and annealed at ∼150 °C for 4 h. Pentacene and PTCDI are thermally evaporated from a Knudsen cell evaporator (Kentax TCE-BSC). Pentacene is thermally evaporated at 156 °C for a few minutes to reach the desired thickness of 0.4 monolayer on the freshly cleaved KBr substrate. The evaporation rate is calibrated with a quartz crystal microbalance before evaporation to reach a stable deposition. PTCDI is evaporated at 300 °C for 1 min to obtain 0.2 monolayer deposited on the KBr substrate.

Pulse Bias Measurement. We implement a pulsed bias technique by holding the tip at a constant height (0 nm tip lift from $\Delta f = -6$ Hz set point) above the pentacene island while a square wave bias pulse is applied by an external function generator to the tip and the frequency shift of the cantilever is recorded for 10 ms with the Nanonis system (PLL bandwidth 100 Hz). The tip oscillation amplitude is set to 6 nm using a Nanosensors PPP-NCHPt cantilever with a resonance frequency of 288 kHz. We apply a 1 V to −8 V (negative) or a 1−4 V (positive) amplitude square wave, while varying the frequency of the pulse (from 1 kHz to 1 MHz), to probe the negative/positive voltage range of Figure 2, respectively. A null experiment is also performed on KBr. The pulse amplitude where chosen for optimal driving to inversion and accumulation, respectively.

ASSOCIATED CONTENT

Supporting Information

The Supporting Information is available free of charge at https://pubs.acs.org/doi/10.1021/acsnano.1c02600.

Details regarding difference map of df/dV, calculation of electrostatic force and frequency shift, additional intrinsic carrier and dopant concentration calculations, forward and backward sweeps of the bias spectroscopy shown in Figure 2, error of the difference in the KPFS map (PDF)

AUTHOR INFORMATION

Corresponding Author

Zeno Schumacher − *Department of Physics, McGill University, Montreal, Quebec H3A 2T8, Canada;* Present Address: (Z.S.) Department of Physics, Institute of Quantum Electronics, ETH Zurich, 8093 Zürich, Switzerland.; orcid.org/0000-0001-6542-7978; Email: zenos@physics.mcgill.ca

https://doi.org/10.1021/acsnano.1c02600
ACS Nano 2021, 15, 10377−10383

Authors

Rasa Rejali − *Department of Physics, McGill University, Montreal, Quebec H3A 2T8, Canada*

Megan Cowie − *Department of Physics, McGill University, Montreal, Quebec H3A 2T8, Canada*

Andreas Spielhofer − *Department of Physics, McGill University, Montreal, Quebec H3A 2T8, Canada*

Yoichi Miyahara − *Department of Physics, McGill University, Montreal, Quebec H3A 2T8, Canada;* Present Address: (Y.M.) Department of Physics, Texas State University, San Marcos, Texas 78666, United States.; orcid.org/0000-0002-9514-9603

Peter Grutter − *Department of Physics, McGill University, Montreal, Quebec H3A 2T8, Canada;* orcid.org/0000-0003-1719-8239

Complete contact information is available at: https://pubs.acs.org/10.1021/acsnano.1c02600

Notes

The authors declare no competing financial interest.

ACKNOWLEDGMENTS

We thank NSERC and FRQNT for funding. Z.S. gratefully acknowledges the SNSF for a DOC.Mobility fellowship.

REFERENCES

(1) Takihara, M.; Takahashi, T.; Ujihara, T. Minority Carrier Lifetime in Polycrystalline Silicon Solar Cells Studied by Photoassisted Kelvin Probe Force Microscopy. *Appl. Phys. Lett.* **2008**, *93*, 021902.

(2) Borowik, Ł.; Lepage, H.; Chevalier, N.; Mariolle, D.; Renault, O. Measuring the Lifetime of Silicon Nanocrystal Solar Cell Photo-Carriers by Using Kelvin Probe Force Microscopy and X-Ray Photoelectron Spectroscopy. *Nanotechnology* **2014**, *25*, 265703.

(3) Loppacher, C.; Zerweck, U.; Teich, S.; Beyreuther, E.; Otto, T.; Grafström, S.; Eng, L. M. FM Demodulated Kelvin Probe Force Microscopy for Surface Photovoltage Tracking. *Nanotechnology* **2005**, *16*, S1−S6.

(4) Shao, G.; Glaz, M. S.; Ma, F.; Ju, H.; Ginger, D. S. Intensity-Modulated Scanning Kelvin Probe Microscopy for Probing Recombination in Organic Photovoltaics. *ACS Nano* **2014**, *8*, 10799−10807.

(5) Hoppe, H.; Glatzel, T.; Niggemann, M.; Hinsch, A.; Lux-Steiner, M. C.; Sariciftci, N. S. Kelvin Probe Force Microscopy Study on Conjugated Polymer/Fullerene Bulk Heterojunction Organic Solar Cells. *Nano Lett.* **2005**, *5*, 269−74.

(6) Hoppe, H.; Glatzel, T.; Niggemann, M.; Schwinger, W.; Schaeffler, F.; Hinsch, A.; Lux-Steiner, M. C.; Sariciftci, N. Efficiency Limiting Morphological Factors of MDMO-PPV:PCBM Plastic Solar Cells. *Thin Solid Films* **2006**, *511*−*512*, 587−592.

(7) Neff, J. L.; Rahe, P. Insights into Kelvin Probe Force Microscopy Data of Insulator-Supported Molecules. *Phys. Rev. B: Condens. Matter Mater. Phys.* **2015**, *91*, 085424.

(8) Luria, J. L.; Hoepker, N.; Bruce, R.; Jacobs, A. R.; Groves, C.; Marohn, J. A. Spectroscopic Imaging of Photopotentials and Photoinduced Potential Fluctuations in a Bulk Heterojunction Solar Cell Film. *ACS Nano* **2012**, *6*, 9392−9401.

(9) Steurer, W.; Fatayer, S.; Gross, L.; Meyer, G. Probe-Based Measurement of Lateral Single-Electron Transfer between Individual Molecules. *Nat. Commun.* **2015**, *6*, 8353.

(10) Sadewasser, S.; Jelinek, P.; Fang, C.-K.; Custance, O.; Yamada, Y.; Sugimoto, Y.; Abe, M.; Morita, S. New Insights on Atomic-Resolution Frequency-Modulation Kelvin-Probe Force-Microscopy Imaging of Semiconductors. *Phys. Rev. Lett.* **2009**, *103*, 266103.

(11) Hudlet, S.; Saint Jean, M.; Roulet, B.; Berger, J.; Guthmann, C. Electrostatic Forces between Metallic Tip and Semiconductor Surfaces. *J. Appl. Phys.* **1995**, *77*, 3308−3314.

(12) Sadewasser, S., Glatzel, T., Eds.; *Kelvin Probe Force Microscopy*; Springer Series in Surface Sciences; Springer International Publishing: Cham, 2018; *Vol. 65*.

(13) Feenstra, R. M.; Dong, Y.; Semtsiv, M. P.; Masselink, W. T. Influence of Tip-Induced Band Bending on Tunnelling Spectra of Semiconductor Surfaces. *Nanotechnology* **2007**, *18*, 044015.

(14) Feenstra, R. M. Electrostatic Potential for a Hyperbolic Probe Tip near a Semiconductor. *J. Vac. Sci. Technol., B: Microelectron. Process. Phenom.* **2003**, *21*, 2080.

(15) Huang, Y.; Slinkman, J.; Williams, C. Modelling of Impurity Dopant Density Measurement in Semiconductors by Scanning Force Microscopy. *Ultramicroscopy* **1992**, *42*, 298−303.

(16) Donolato, C. Electrostatic Tip-Sample Interaction in Immersion Force Microscopy of Semiconductors. *Phys. Rev. B: Condens. Matter Mater. Phys.* **1996**, *54*, 1478−1481.

(17) Schwarz, A.; Allers, W.; Schwarz, U. D.; Wiesendanger, R. Detection of Doping Atom Distributions and Individual Dopants in InAs(110) by Dynamic-Mode Scanning Force Microscopy in Ultrahigh Vacuum. *Phys. Rev. B: Condens. Matter Mater. Phys.* **2000**, *62*, 13617−13622.

(18) Neff, J. L.; Milde, P.; León, C. P.; Kundrat, M. D.; Eng, L. M.; Jacob, C. R.; Hoffmann-Vogel, R. Epitaxial Growth of Pentacene on Alkali Halide Surfaces Studied by Kelvin Probe Force Microscopy. *ACS Nano* **2014**, *8*, 3294−301.

(19) Topple, J. M.; Burke, S. A.; Ji, W.; Fostner, S.; Tekiel, A.; Grütter, P. Tailoring the Morphology and Dewetting of an Organic Thin Film. *J. Phys. Chem. C* **2011**, *115*, 217−224.

(20) Rost, C.; Gundlach, D. J.; Karg, S.; Rieß, W. Ambipolar Organic Field-Effect Transistor Based on an Organic Heterostructure. *J. Appl. Phys.* **2004**, *95*, 5782−5787.

(21) Ahles, M.; Schmechel, R.; von Seggern, H. *n*-Type Organic Field-Effect Transistor Based on Interface-Doped Pentacene. *Appl. Phys. Lett.* **2004**, *85*, 4499−4501.

(22) Lüssem, B.; Tietze, M. L.; Kleemann, H.; Hoßbach, C.; Bartha, J. W.; Zakhidov, A.; Leo, K. Doped Organic Transistors Operating in the Inversion and Depletion Regime. *Nat. Commun.* **2013**, *4*, 2775.

(23) Nicollian, E. H.; Brews, J. R. *MOS (Metal Oxide Semiconductor) Physics and Technology*; John Wiley & Sons, Inc.: New York, 2002.

(24) Wang, H.; Wang, J.; Yan, X.; Shi, J.; Tian, H.; Geng, Y.; Yan, D. Ambipolar Organic Field-Effect Transistors with Air Stability, High Mobility, and Balanced Transport. *Appl. Phys. Lett.* **2006**, *88*, 133508.

(25) Zerbst, M. Relaxationseffekte an Halbleiter-Isolator-Grenzflachen. *Z. Angew. Phys.* **1966**, *22*, 30.

(26) Heiman, F. On the Determination of Minority Carrier Lifetime from the Transient Response of an MOS Capacitor. *IEEE Trans. Electron Devices* **1967**, *14*, 781−784.

(27) Schroder, D.; Nathanson, H. On the Separation of Bulk and Surface Components of Lifetime Using the Pulsed MOS Capacitor. *Solid-State Electron.* **1970**, *13*, 577−582.

(28) Schroder, D. Bulk and Optical Generation Parameters Measured with the Pulsed MOS Capacitor. *IEEE Trans. Electron Devices* **1972**, *19*, 1018−1023.

(29) Hillen, M.; Girisch, R. The Influence of Surface States on a Pulsed MOS Capacitor Recombination Lifetime Measurement. *Solid-State Electron.* **1980**, *23*, 189−195.

(30) Zhang, X.; Ding, K. Capacitance-Time Transient Characteristics of Pulsed MOS Capacitor Application in Measurement of Semiconductor Parameters. *IEE Proceedings G Circuits, Devices and Systems* **1993**, *140*, 449.

(31) Stomp, R.; Miyahara, Y.; Schaer, S.; Sun, Q.; Guo, H.; Grutter, P.; Studenikin, S.; Poole, P.; Sachrajda, A. Detection of Single-Electron Charging in an Individual InAs Quantum Dot by Noncontact Atomic-Force Microscopy. *Phys. Rev. Lett.* **2005**, *94*, 056802.

(32) Cockins, L.; Miyahara, Y.; Bennett, S. D.; Clerk, A. A.; Studenikin, S.; Poole, P.; Sachrajda, A.; Grutter, P. Energy Levels of

Few-Electron Quantum Dots Imaged and Characterized by Atomic Force Microscopy. *Proc. Natl. Acad. Sci. U. S. A.* **2010**, *107*, 9496−9501.

(33) Fatayer, S.; Albrecht, F.; Zhang, Y.; Urbonas, D.; Peña, D.; Moll, N.; Gross, L. Molecular Structure Elucidation with Charge-State Control. *Science* **2019**, *365*, 142−145.

(34) Ardhuin, T.; Guillermet, O.; Gourdon, A.; Gauthier, S. Measurement and Control of the Charge Occupation of Single Adsorbed Molecules Levels by STM and Nc-AFM. *J. Phys. Chem. C* **2019**, *123*, 26218−26225.

https://doi.org/10.1021/acsnano.1c02600
ACS Nano 2021, 15, 10377−10383